Contents lists available at ScienceDirect

Chemical Engineering Research and Design

journal homepage: www.elsevier.com/locate/cherd

Operational safety of an ammonia process network via model predictive control

Zhihao Zhang[a], Zhe Wu[a], David Rincon[a], Panagiotis D. Christofides[a,b,*]

[a] Department of Chemical and Biomolecular Engineering, University of California, Los Angeles, CA 90095-1592, USA
[b] Department of Electrical and Computer Engineering, University of California, Los Angeles, CA 90095-1592, USA

ARTICLE INFO

Article history:
Received 9 March 2019
Received in revised form 31 March 2019
Accepted 2 April 2019
Available online 19 April 2019

Keywords:
Operational safety
Process control
Model predictive control
Nonlinear processes
Ammonia process

ABSTRACT

Process safety is a crucial issue in the area of process systems engineering as accident prevention is a top priority in process operations. Operational safety needs to be directly incorporated into control system design to handle disturbances in the process. Motivated by the above considerations, this paper presents a practical application simulating multiple model predictive controllers within a multi-unit ammonia process, all of which integrate safety constraints of the process within their design. Specifically, catalytic deactivation in the shift reactor is a common and problematic disturbance that may trigger reaction thermal runaway in the methanator. Two controllers designed with the objective of improving operational safety are implemented on the ammonia plant under catalyst deactivation. Aspen Plus is a commercial process simulation software which is integrated with Matlab to run a closed-loop simulation for the ammonia process. The results demonstrate that under suitable design of the controllers, desirable closed-loop performance is achieved with high temperature extremities avoided during operation.

1. Introduction

Given the intrinsic inter-connectivity of different process units in chemical industries, proper control strategies need to be carefully considered during the design phase, and rigorously practiced during regular operations, in order to maintain consistent operating conditions and high plant productivity. The ammonia plant is one example of a highly interconnected system that produces mainly chemical fertilizers to enhance food production. Due to increase of population and changing consumption patterns, the production of ammonia has increased as well (Luyben, 2018). For instance, the global production of ammonia is estimated to be 200 t/year (Nayak-Luke et al., 2018). However, the increase of ammonia production also brings new challenges that have not been fully tackled. For example, traditionally the safety of the ammonia plant is studied by analyzing each individual unit of the process, and then various process safety metrics and methodologies (e.g., Hazard and Operability Analysis (HAZOP), Layer of Protection Analysis (LOPA)) are implemented before the process goes online in order to avoid potential process upsets and safety hazards (Pattabathula and Richardson, 2016; Albalawi et al., 2018). The traditional control methodologies are unaware of important safety conditions of the ammonia process.

Since the ammonia plant operates under considerable high temperatures and pressures, it is well known that the variation from the operation point can damage the equipment and impact the safety and profitability of the process. For instance, failures and pitfalls in the ammonia process have been reported in the literature (e.g., Ojha and Dhiman (2010)). It has been pointed out in Campbell (1970) that operators are conscious of the impact of the die-off in the low-temperature shift reactor. The die-off has been mitigated by studying the correct selection of the catalyst and by reducing the impurities

* *Corresponding author at*: Department of Chemical and Biomolecular Engineering, University of California, Los Angeles, CA 90095-1592, USA.
E-mail address: pdc@seas.ucla.edu (P.D. Christofides).
https://doi.org/10.1016/j.cherd.2019.04.004

that cause the loss of activity or catalyst poisoning. Similarly, since cleaning the poisoned catalysts requires 12–24 h in a high-temperature shift reactor, the wasted production time is an important factor to be considered (Rounthwaite, 1983). In order to increase the catalyst life without stopping the process, it is usual practice to implement a small increase in pressure drop in the low-temperature shift reactor, which leads to the loss of ammonia production and to the loss of thousands of dollars. The poisoning of the catalyst and other disturbances in the high-temperature shift converter have also been associated with triggering the runaway reaction in the methanator (Alhabdan and Elnashaie, 1995). Similarly, overheating in the methanation vessel that was caused by electrical power failure or by the failure in the heat boiler has been also reported in the ammonia industry under an already existing high-temperature protection system (Ocampo, 1996; Walton et al., 2009). It was detected that the high-temperature protection system failed because the fast increase of the temperature happened between measurements (Walton et al., 2009).

There are limited research efforts on process safety and control in the ammonia process. Despite the importance of real-time operational safety considerations, most works focus on the modeling and steady-state issues of safety in the ammonia plant (Shah, 1967; Shah and Weisenfelder, 1969; Araújo and Skogestad, 2008; Zhang et al., 2010; Luyben, 2018). One research work (Luyben, 2012) reports the introduction of two failures in an ammonia plant with a plant-wide control structure: loss of coolant in the reactor, and loss of cooling water in the condenser (Luyben, 2012). To tackle the above safety issues, an override control structure was implemented and simulated in Aspen Plus Dynamics. In another research work, the control performance of the ammonia synthesis process was improved by updating the control loops and it was pointed out that further improvement can be achieved via a multi-variable predictive control system (Domanski et al., 2016).

Studies that evaluate the hazards and safety in real-time operation of a multi-unit ammonia process are also limited in the literature. For example, the ammonia process was studied in Aspen HYSYS environment with the hazard and operability (HAZOP) methodology (Janošovský et al., 2017). From the HAZOP analysis of this study, it was concluded that the reaction conversion is too low when pressure and feed temperature are below 70% and 18% of the operation point, respectively. Another methodology available is the master logic diagram (MLD) technique that identifies the initiating event of a hazard. The MLD technique was implemented in an ammonia storage facility, and it was concluded that the most relevant initiating events are excess external heat, earthquakes, and loss of refrigeration capacity, among many others (Papazoglou and Aneziris, 2003). More recently in a different industry, an evaluation approach called multi-unit probabilistic risk assessment (MUPRA), has been proposed to account for the interaction between systems (Zhang et al., 2016). The key point of the MUPRA methodology is to assess the risk as an interacting multi-unit system rather than one single unit. However, the implementation of the MUPRA methodology is still offline.

In terms of coordinating control with safety considerations, the existing techniques usually tackle the safety problem as fault identification (Mhaskar et al., 2013; Lao et al., 2013; Bø and Johansen, 2014). However, the case when the safety system actions and the control actions are integrated and respond to the hazardous disturbances in real time has received attention only recently. To address the above problem, recent works have started to explore how to reduce the gap between the control system and the safety considerations. For instance, model predictive control (MPC) and economic model predictive control (EMPC) approaches were proposed to drive the process to safe operating regions using secure interior level sets (Albalawi et al., 2016, 2018). In order to characterize the safe region of operation, Safeness Index was proposed to indicate safeness of the process based on process state information (Albalawi et al., 2017). On the other hand, the control Lyapunov-Barrier function was introduced as a constraint in the MPC formulation to avoid unsafe condition and to ensure stability (Wu et al., 2018). Finally, the practical integration of the safety system with a control system was demonstrated in two relevant examples from literature: the MIC reactor and a high-pressure flash drum separator (Zhang et al., 2018).

Motivated by the above considerations, the main contribution of this paper is to design a safety control scheme that integrates process operational safety and control for a multi-unit ammonia process network. Specifically, an industrial case study of a multi-unit ammonia process is studied and a control scheme is proposed and applied to an ammonia process under a disturbance that is typically encountered by engineers in practice. Under the disturbance of loss of catalyst activity in the first unit in the proposed ammonia plant, the gas temperature and concentration in the last methanation unit are affected, which could lead to unsafe operation of the whole process. To improve process operational safety in the ammonia process, two controllers on high-temperature shift reactor and methanator are designed. Specifically, the first controller is a tracking model predictive controller and the second controller is a Safeness Index-based model predictive controller. Finally, the closed-loop simulations of the ammonia plant are performed in a co-simulation between Matlab and Aspen Plus Dynamics.

The rest of the paper is organized as follows: in Section 2, the implemented ammonia process, the setting in Aspen Plus Dynamics and the process disturbance are presented. In Section 3, the designed control scheme and the model predictive control structures are presented. In Section 4, the proposed controllers are applied to the ammonia plant in the presence of disturbances to evaluate the closed-loop performance.

2. Ammonia process and dynamic simulation

In this section, a simplified description of the ammonia process is presented together with the key points of each unit in the ammonia process. Specifically, the ammonia process is generally developed based on the followings steps: feed stock pretreatment, steam reforming, gas purification, compression, and ammonia synthesis (Appl, 2000). A schematic of the entire ammonia process network is shown in Fig. 1. This paper focuses specifically on the gas purification step, within which three sub-processes are simulated: shift conversion, carbon dioxide removal, and methanation. The common purpose of all three sub-processes within gas purification is to remove carbon monoxide and carbon dioxide produced by the previous steam reforming step. Fig. 2 shows the schematic of the ammonia process implemented in this paper, where HT-shift, LT-shift, and HE stand for high-temperature shift reactor, low-temperature shift reactor, and heat exchanger, respectively.

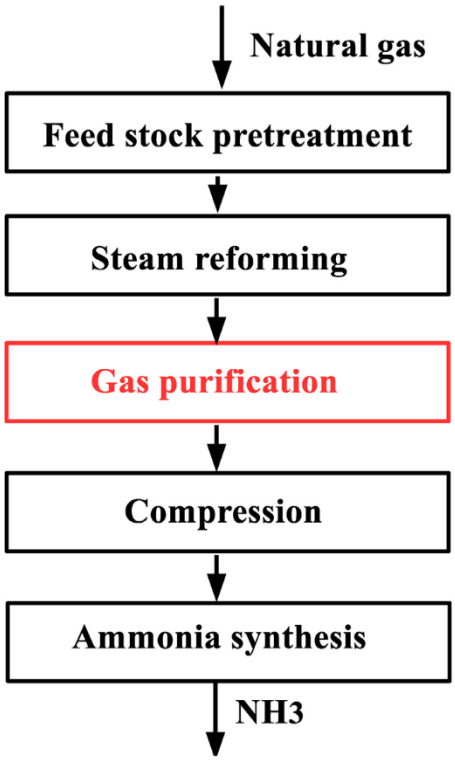

Fig. 1 – A schematic of the entire ammonia process network.

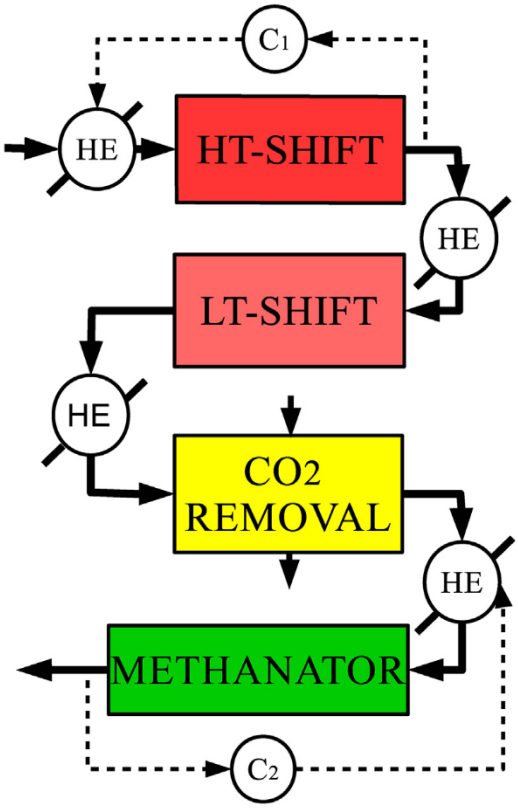

Fig. 2 – A schematic of the control structure that uses two control loops, where C_1 and C_2 represent controller 1 and controller 2.

In the shift conversion section, two-bed adiabatic operation is used to eliminate the carbon monoxide. Each bed operates at different temperatures (i.e., 400 °C and 200 °C, respectively) with different catalyst components. An exothermic reaction is carried out in each reactor between carbon monoxide and water to yield carbon dioxide and hydrogen. In the high-temperature shift reactor, large amount of carbon monoxide is removed due to its high temperature and the resulting high reaction rate. In the low-temperature shift reactor, carbon monoxide is further removed by reacting at relatively low temperature because the equilibrium is preferred at low temperature in the exothermic reversible reaction. According to Appl (2000); Twigg (1989); Ettouney et al. (1995), the high-temperature shift reactor should reduce the carbon monoxide to 2–4% under normal operating conditions, and the low-temperature shift reactor should further reduce carbon monoxide into the range of 0.1–0.3%.

In the two shift reactors, a surplus amount of water vapor is introduced into the gas stream and a large amount of carbon dioxide is produced. Water vapor and carbon dioxide are afterwards removed in an adsorption column, which otherwise will poison the ammonia synthesis catalyst (Appl, 2000). Additionally, the gas is purified in the adsorption column by using different kinds of solvent. In general, the most typical absorption processes are classified as follows: reaction systems (e.g., Benfield), combination reaction-physical systems (e.g., Sulfinol), and physical absorption systems (e.g., Selexol) (Czuppon et al., 1992).

Finally, after the gas leaves the adsorption column, trace amount of carbon monoxide and carbon dioxide are still present in the stream. A catalytic methanation reaction unit is used to remove the trace amount of carbon monoxide and carbon dioxide. Two exothermic catalytic reactions are carried out in the adiabatic tubular methanation reactor and transform the remaining carbon monoxide and carbon dioxide with hydrogen into methane and water (Rönsch et al., 2016; Martínez et al., 2017). This methanation unit is also known for being challenging due to the high heat generation of reaction and sensitivity to the catalyst (Rönsch et al., 2016). A thermal runaway can occur in methanator in the case that disturbance is introduced in upstream shift conversion reactors (Alhabdan and Elnashaie, 1995). Finally, the methanation unit is expected to reduce concentrations of carbon monoxide and carbon dioxide to 0.0005–0.001% (Twigg, 1989; Ojha and Dhiman, 2010).

2.1. *Simulation settings in Aspen Plus*

In order to accurately simulate the process dynamics and interaction among units, Aspen Plus and Aspen Plus Dynamics V10.0 (Aspen Technology, Inc.) are used to perform high-fidelity dynamic simulation of gas purification process within the ammonia process. Aspen Plus is a commercial software that calculates the steady-state of the process given a process design and an appropriate selection of thermodynamic models, based on the mass and energy balances of the process using a sequential modular approach. Aspen Plus Dynamics is another software that can run dynamic simulations based on steady-state model data and additional detailed parameters. Further details about Aspen software can be found in Al-Malah (2016); Aspen Technology, Inc. (2003).

In our simulation, involved components are carefully chosen and the Redlich Kwong Soave Boston Mathias (RKS-BM) model was selected for the thermodynamic property calculation of all involved chemical components. A steady-state model is first built in Aspen Plus based on the detailed information in the example provided by Aspen (Aspen Technology, Inc., 2017). Subsequently, the obtained steady-state model in Aspen Plus is exported to a dynamic model in Aspen Plus

Dynamics, which is a software that can conduct dynamic process simulations. We first validate the model configuration using the Pressure Checker Tool, and then export the steady-state model to a pressure-driven dynamic file using the Dynamic Mode Tool.

Gas phase reactions in all units are modeled using the reaction rate equations from Ettouney et al. (1995); Aspen Technology, Inc. (2017). Since the kinetic models available in Aspen Plus are limited, it is necessary to adopt a user-defined routine for complex kinetic models. In our work, the reaction rate equations are programmed in a FORTRAN user-kinetics subroutine file, and then the FORTRAN code is compiled into object file and linked to the Aspen Plus software as a dynamic link library file. Specifically, the reaction rate equations for the selected three units (i.e., high-temperature shift reactor and low-temperature shift reactor, and methanator) and the relevant parameters are discussed in Zhang et al. (2019) and given as follows:

High-temperature shift reaction: $CO + H_2O \rightleftarrows CO_2 + H_2$, $\Delta H = -41.2$ kJ/mol:

$$r_{CO} = -A_c \exp\left(-\frac{300.69}{T} + 8.02\right)(P)^{1/2}\left(y_{CO} - \frac{y_{H_2} y_{CO_2}}{K_{eq} y_{H_2O}}\right),$$
$$K_{eq} = \exp\left(\frac{8240}{T} - 4.33\right) \quad (1)$$

Low-temperature shift reaction: $CO + H_2O \rightleftarrows CO_2 + H_2$, $\Delta H = -41.2$ kJ/mol:

$$r_{CO} = -A_c \frac{513.15}{T} \frac{K_L y_{CO} y_{H_2O}^{1/2}\left(1 - \frac{K}{K_{eq}}\right)}{\frac{1}{P} + K_A y_{CO} + K_B y_{CO_2}},$$
$$K = \frac{y_{H_2} y_{CO_2}}{y_{CO} y_{H_2O}}, \quad K_{eq} = \exp\left(\frac{8240}{T} - 4.33\right)$$
$$K_L = 68.4 \exp\left(-3620\left(\frac{1}{513.15} - \frac{1}{T}\right)\right), \quad (2)$$
$$K_A = 4.31 \exp\left(-4580\left(\frac{1}{513.15} - \frac{1}{T}\right)\right),$$
$$K_B = 1.35 \exp\left(-1500\left(\frac{1}{513.15} - \frac{1}{T}\right)\right)$$

Methanation reaction 1: $CO + 3H_2 \rightleftarrows CH_4 + H_2O$, $\Delta H = -206$ kJ/mol:

$$r_{CO} = -A_c \quad 3.119 \quad \exp\left(1300\left(\frac{1}{T} - \frac{1}{513}\right)\right) \quad \left(\frac{P}{y_{H_2}}\right)^{1/2}$$
$$\left(y_{CO} - \frac{y_{CH_4} \quad y_{H_2O}}{y_{H_2}^3 \quad P^2 \quad \exp\left(-38.4523 + \frac{2627}{T}\right)}\right) \quad (3)$$

Methanation reaction 2: $CO_2 + 4H_2 \rightleftarrows CH_4 + 2H_2O$, $\Delta H = -164$ kJ/mol:

$$r_{CO} = -A_c \quad 3.119 \quad \exp\left(1300\left(\frac{1}{T} - \frac{1}{513}\right)\right) \quad \left(\frac{P}{y_{H_2}}\right)^{1/2}$$
$$\left(y_{CO_2} - \frac{y_{CH_4} \quad y_{H_2O}^2}{y_{H_2}^4 \quad P^2 \quad \exp\left(-38.4523 + \frac{2627}{T}\right)}\right) \quad (4)$$

In our simulation, pressure and flow rate of each unit are carefully tuned by adjusting the feed pressure and pressure drop of each unit. All heat exchangers work at fixed outlet temperature with varying heating duty. The values of the main parameters and steady-states for all implemented units are shown in Table 1. Below we discuss the key design issues in the main units.

In the high-temperature shift reactor, the size and catalyst properties are designed according to Aspen Technology, Inc. (2017); Alhabdan and Elnashaie (1995); Twigg (1989); Ettouney et al. (1995). There exists an optimal feed temperature because high temperature can increase reaction rate while low temperature can lead to a better equilibrium in the case of exothermic reversible reaction (Seo et al., 2006; Rahimpour et al., 2012). In this unit, the optimal feed temperature is determined by evaluating different feed temperatures in the simulation and then selecting the one with the highest conversion of carbon monoxide. Our results are consistent with industrial data.

In the low-temperature shift reactor, the length and the diameter of the reactor, as well as the characteristics of the catalyst are found in Aspen Technology, Inc. (2017); Alhabdan and Elnashaie (1995); Twigg (1989); Ettouney et al. (1995). Due to low feed concentration, different catalyst and reactor size, the optimal feed temperature for low-temperature shift reactor can be very low. However, the limiting condition is the dew point of the gas because condensed water on catalyst is poisonous. Analysis tool for mixture in the Properties sheet in Aspen Plus is used to find the dew point to be 169 °C for the specific high pressure and high temperature gas, and 210 °C is chosen according to industrial data (Aspen Technology, Inc., 2017; Alhabdan and Elnashaie, 1995; Ettouney et al., 1995).

In the carbon dioxide removal unit, an aqueous ammonia solution is used to remove carbon dioxide as well as to condense water from gas phase. In our simulation, a flash drum is chosen to represent the adsorption column unit. The gas from shift reactor is cooled down to 40 °C, and fed into flash drum. Meanwhile a stream of ammonia (15%) and water (85%) is also fed into the flash drum. Gas leaves flash drum with removal rates 98.6% and 99.7% for carbon dioxide and water, respectively. Detailed electrolyte solution chemistry properties and reaction kinetic in CO_2 removal are discussed in Aspen Technology, Inc. (2017); Kohl and Nielsen (1997).

The gas is heated up after the carbon dioxide removal unit, and then fed into the methanation unit to apply the final purification step. Feed temperature is chosen to be 280 °C such that final outlet CO and CO_2 mole fraction is below 0.0005%. The characteristic values of the equipment and other key values of the methanator are carefully chosen according to the data from Twigg (1989); Rönsch et al. (2016); Khorsand et al. (2007).

2.2. *Disturbance and process operational safety*

One of the most common safety issues that is encountered in the ammonia plant is runaway reactions caused by catalyst deactivation in shift reactors (Argyle and Bartholomew, 2015; Alhabdan and Elnashaie, 1995, 1995; Walton et al., 2009). In the operation of the ammonia process, the disturbance of catalyst deactivation affects the process in the following way as demonstrated in Fig. 3. First, the catalyst activity starts to decrease in the high-temperature shift reactor and less CO is consumed. Second, the low-temperature shift reactor buffers the increasing CO content, but CO concentration still increases considerably. Third, no CO is removed in the CO_2 removal

Table 1 – Key parameters of the ammonia process.

Feed	Temperature 980 °C Mole fraction y_{CO_2} 0.0507	Pressure 29 bar Mole fraction y_{H_2} 0.355	Molar flowrate 3435 mol/s Mole fraction y_{H_2O} 0.353	Mole fraction y_{CO} 0.0839 Mole fraction y_{N_2} 0.152
HT-shift	Reactor length 15.8 m Catalyst heat capacity 900 J/kg K	Reactor diameter 4.4 m Feed temperature 360 °C	Loaded catalyst 9.61×10^4 kg	Voidage 0.5
LT-shift	Reactor length 7.7 m Catalyst heat capacity 850 J/kg K	Reactor diameter 3.7 m Feed temperature 210 °C	Loaded catalyst 3.48×10^4 kg	Voidage 0.5
CO_2 Removal	Volume 49.09 m^3 H_2O removal rate 99.7%	Temperature 30 °C	Pressure 26.9 bar	CO_2 removal rate 98.6%
Methanator	Reactor length 4 m Catalyst heat capacity 900 J/kg K	Reactor diameter 2.5 m Feed temperature 280 °C	Loaded catalyst 1.57×10^4 kg	Voidage 0.5

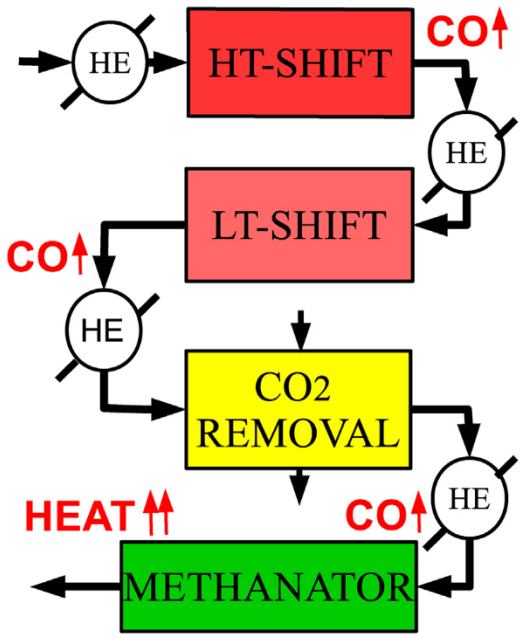

Fig. 3 – A schematic of disturbance propagation from high-temperature shift reactor to methanator, where increasing concentration of CO will lead to higher temperatures in the methanator that may trigger reaction thermal runaway.

unit, and therefore more CO goes into the methanator as reactant. Finally, more CO undergoes an exothermic reaction in the methanator which leads to a drastic increase in temperature. As an example of this phenomenon, Fig. 4 shows an open-loop simulation of the methanator when the catalyst activity is decreasing from 1 to 0.2 in 300 s. As a result of this disturbance, the outlet temperature increases from 330 °C to 390 °C in the methanator.

3. Feedback controller design

3.1. Control scheme

In order to avoid unsafe operation in the case of decreasing catalyst activity, a model predictive controller with feedforward term is implemented in ammonia process in Zhang et al. (2019). In order to further improve operational safety, in this paper two controllers are designed for the high-temperature shift reactor and methanator, respectively. The first controller (C_1) is added on the high-temperature shift reactor. The control variable of the first controller is the reactor outlet temperature and the manipulated variable is the reactor inlet temperature, which is actuated by a heat exchanger. The second controller (C_2) is added on the methanator. The control variable of the second controller is the methanator outlet temperature and the manipulated variable is the methanator inlet temperature, which is actuated by another heat exchanger. It needs to be mentioned that the gas temperature inside the reactor is a crucial process variable to monitor operational safety and it increases monotonously from inlet to outlet in both high-temperature shift reactor and methanator. Therefore, outlet temperature is a reliable variable to indicate unsafe reactor operation. The described control loops in the ammonia process are demonstrated in Fig. 2.

3.2. High-temperature shift reactor controller

In the high-temperature shift reactor, less reaction occurs in the tube when the catalyst activity decreases, which leads to a decrease of reactor outlet temperature. In order to increase reaction rate and consume more carbon monoxide, the inlet temperature needs to be increased by adjusting the heat exchanger. To this end, a model predictive controller (MPC) is designed for the high-temperature shift reactor by manipulating the inlet temperature to control the outlet temperature. Since the process model in MPC is identified from the nominal process, to mitigate the effect of model mismatch, an integral term is added on the control action calculated by MPC to eliminate offset.

3.2.1. Model identification

The high-temperature shift reactor is initially simulated at its steady-state where feed temperature $T_{1,in,ss} = 360\,°C$ and outlet temperature $T_{1,out,ss} = 429.18\,°C$. The state and the input of the process are represented in deviation variable form as $x_1 = T_{1,out} - T_{1,out,ss}$, $u_1 = T_{1,in} - T_{1,in,ss}$, such that the equilibrium point of the system is at the origin.

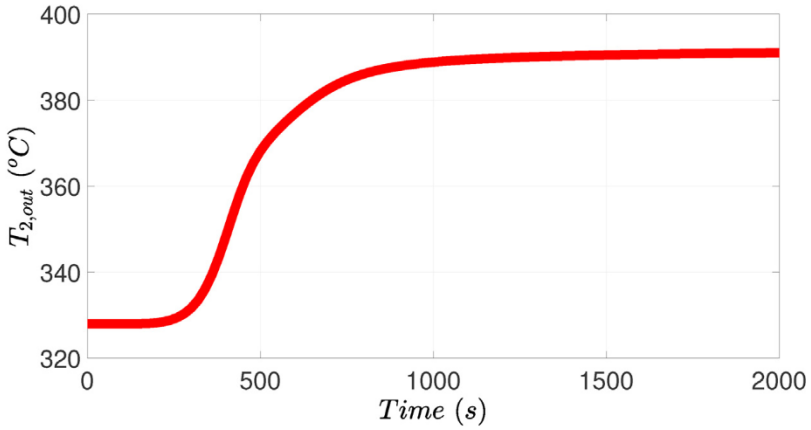

Fig. 4 – Methanator outlet temperature profile under open-loop simulation, where the temperature increases from 330 °C to 390 °C after catalyst activity in the high-temperature shift reactor decreases from 1 to 0.2 in 300 s.

It is observed that there is an inverse response between the feed temperature $T_{1,in}$ and the outlet temperature $T_{1,out}$ for the high-temperature shift reactor. The reason is that for an adiabatic exothermic tube reactor, a drop in the inlet temperature causes a reduced reaction rate at the cooler upstream part of the tube reactor. Thus, the gas stream entering the downstream part of the tube reactor has a higher CO concentration, which speeds up the reaction in the downstream part of the tube reactor. This leads to a temporary increase in the local heat generation at the reactor outlet. However, the outlet temperature will decrease ultimately due to the decrease of inlet temperature (Van Dijk et al., 2010; Peng et al., 2017).

Since the effect of inverse response is negligible, inverse response is treated as time delay. Thus a linear dynamic model with time delay of the following form is utilized for the high-temperature shift reactor:

$$\frac{dx_1(t)}{dt} = A_1 x_1(t) + B_1 u_1(t - t_{d,1}) \tag{5}$$

where $t_{d,1}$ is the time delay in seconds. Aspen open-loop simulation is used to generate transient response data of the outlet temperature $T_{1,out}$ subject to a step change in feed temperature $T_{1,in}$, and Multivariable Output Error State Space (MOSEP) algorithm is applied in Matlab to identify the matrices A_2 and B_2. The matrices A_1, B_1 and the time delay $t_{d,1}$ are identified as follows:

$$A_1 = -0.015; \quad B_1 = 0.0142; \quad t_{d,1} = 360\,\text{s}$$

3.2.2. C_1 design via MPC

The first controller is the MPC with an integral term. Specifically, the control action $u_1(t_k)$ consists of an integral term $u_{1,integral}(t_k)$ and an MPC term $u_{1,MPC}(t_k)$, where $u_{1,integral}(t_k)$ is calculated by Eq. (7) and $u_{1,MPC}(t_k)$ is the first control action in the solution $u^*(t)$ to the optimization problem of Eq. (8). Specifically,

$$u_1(t_k) = u_{1,MPC}(t_k) + u_{1,integral}(t_k) \tag{6}$$

$$e(t_k) = T_{1,out,set} - T_{1,out}(t_k)$$
$$u_{integral}(t_k) = \frac{1}{\tau_I}\int_0^{t_k} e(\tau)\ d\tau \tag{7}$$

and

$$\min_{u\in S(\Delta),y} \int_{t_k+t_{d,1}}^{t_{k+N}+t_{d,1}} (\|\tilde{x}_1(\tau)\|^2_{Q_c})\ d\tau + \int_{t_k}^{t_{k+N}} (\|u_1(\tau)\|^2_{R_c})\ d\tau \tag{8a}$$

$$\text{s.t.} \quad \dot{\tilde{x}}_1(t) = A_1\tilde{x}_1(t) + B_1 u_1(t - t_{d,1}) \tag{8b}$$

$$\tilde{x}_1(t_k) = x_1(t_k) \tag{8c}$$

$$u_1(t) = u_{1,pre}(t), \quad \forall t \in [t_k - t_{d,1}, t_k) \tag{8d}$$

$$u_1(t) \in U_1, \quad \forall t \in [t_k, t_{k+N}) \tag{8e}$$

The objective function of Eq. (8a) requires minimizing the terms $\int_{t_k+t_{d,1}}^{t_{k+N}+t_{d,1}}(\|\tilde{x}_1(\tau)\|^2_{Q_c})\ d\tau$ and $\int_{t_k}^{t_{k+N}}(\|u_1(\tau)\|^2_{R_c})\ d\tau$ so that the system can be driven to its steady-state. The constraint of Eq. (8b) is the nominal linear model of Eq. (5) that is used to predict future states. Eq. (8c) defines the initial condition $\tilde{x}_1(t_k)$ of the optimization problem as the state measurement $x_1(t_k)$ at $t = t_k$. Eq. (8d) provides input trajectory calculated from previous steps, in order to predict the state from t_k to $t_k + t_{d,1}$. Eq. (8e) is the input constraint applied over the entire prediction horizon. The manipulated input is the feed temperature $T_{1,in}$, which is bounded by: 310 °C ≤ $T_{1,in}$ ≤ 410 °C, namely $U_1 = [-50, 50]$.

The explicit Euler method with an integration time step of $h_c = 10^{-1}$ s is applied to numerically integrate the dynamic model of Eq. (8b) in MPC. The nonlinear optimization problem of MPC of Eq. (8) is solved using the solver FilterSD on OPTI Toolbox in Matlab with the following parameters: sampling period $\Delta = 20$ s; prediction horizon $N = 30$. $Q_c = 1$ and $R_c = 0.2$ are chosen such that the terms of the states and the input have the same order of magnitude in $\|\tilde{x}_1(\tau)\|^2_{Q_c}$ and $\|u_1(\tau)\|^2_{R_c}$. The integral time constant $\tau_I = 33.3$ s is determined to eliminate the offset of the closed-loop system without oscillation.

3.3. Methanator controller

Although the low-temperature shift reactor mitigates the increase in CO concentration from the high-temperature shift reactor, a higher concentration of CO still reaches the methanator. Since more CO is fed as reactant into the methanator, the temperature increases in the methanator. To avoid potential high temperature in the methanator, a second model predictive controller (MPC) is designed to control

the methanator outlet temperature by manipulating its inlet temperature.

3.3.1. Model identification

The methanator is initially simulated at the steady-state where feed temperature $T_{2,in,ss}$ = 280 °C and outlet temperature $T_{2,out,ss}$ = 327.98 °C. Because the feed *CO* concentration has a dominating effect on the produced heat, the *CO* mole fraction y_{CO} is treated as a measurable disturbance d_2 with a steady-state value of $y_{CO,ss} = 3.55 \times 10^{-3}$, where the deviation variable is $d_2 = y_{CO} - y_{CO,ss}$.

Since increasing feed *CO* content significantly changes the working condition of the methanator, the steady-state of the methanator changes with variation of feed *CO* mole fraction. Therefore, a set of steady-state values of the methanator is calculated offline as a function of feed *CO* mole fraction y_{CO}. Specifically, future inlet temperature and outlet temperature steady-states are expressed as a function of disturbance d_2 as follows:

$$\begin{aligned} &\Delta d = d_2(t_k) - d_2(t_{k-1}) \\ &T(t_{k+N})_{2,in,ss} = 280 - 4080.7(d_2 + \gamma \Delta d N) \\ &T(t_{k+N})_{2,out,ss} = 327.27 + 1616.3(d_2 + \gamma \ \ \Delta d \ \ N) \end{aligned} \tag{9}$$

where $\gamma = 0.5$ is the coefficient to regulate changing speed of future disturbance. If current disturbance $d_2(t_k)$ increases by Δd compared to the disturbance $d_2(t_{k-1})$ at the previous step, future disturbance is anticipated to increase by $\gamma \Delta d$ at each subsequent sampling time, and future steady-state should change accordingly with future disturbance. The above steady-state values are reasonable working conditions obtained offline, where the corresponding outlet *CO* content is below 5×10^{-6} and the outlet temperature is below 340 °C if the disturbance d_2 is not large.

The state and the input of the process are represented in deviation variable form as $x_2 = T_{2,out} - T_{2,out,ss}$ and $u_2 = T_{2,in} - T_{2,in,ss}$ such that the equilibrium point of the system is at zero. Since the transient response of the outlet temperature $T_{2,out}$ has a time delay under a step-change of the feed temperature $T_{2,in}$, a linear dynamic model with time delay of the following form is utilized to represent the Aspen Plus model of the methanator:

$$\frac{dx_2(t)}{dt} = A_2 x_2(t) + B_2 u_2(t - t_{d,2}) \tag{10}$$

where $t_{d,2}$ is the time delay in seconds. Aspen open-loop simulations for the nominal system are used to generate transient response data of the outlet temperature $T_{2,out}$ subject to various step changes in feed temperature $T_{2,in}$, and Multivariable Output Error State Space (MOSEP) algorithm is applied in Matlab to identify the matrices *A* and *B*. Since the disturbance of feed *CO* content changes only the steady-state of the methanator, and barely the dynamics of methanator (i.e., time constant, gain and time delay), the model of Eq. (10) is demonstrated to work well for all steady-states corresponding to different feed *CO* content. The matrices A_2, B_2 and the time delay $t_{d,2}$ are identified as follows:

$$A_2 = -0.005136; \quad B_2 = 0.01207; \quad t_{d,2} = 100\,\text{s}$$

3.3.2. C_2 design via Safeness Index-based MPC

The methanator controller is developed to ensure process operational safety of the ammonia process since high outlet temperature above the steady-state value could lead to unsafe operations. Specifically, Safeness Index is developed and incorporated as a constraint in MPC due to safety considerations in the methanator, meanwhile C_1 is a tracking MPC without explicit safety constraints since there are no critical safety issues in the high-temperature shift reactor. In our work, the Safeness Index is designed such that the process is considered unsafe when the methanator outlet temperature $T_{2,out}$ is above the steady-state operating condition $T_{2,out,ss}$, and safe when the temperature $T_{2,out}$ is below the steady-state value $T_{2,out,ss}$. To that end, we define a function $f^+(x)$ as shown in Eq. (11):

$$f^+(x) = \begin{cases} x, & \text{if} \quad x \geq 0 \\ 0, & \text{if} \quad x < 0 \end{cases} \tag{11}$$

Based on Eq. (11), the Safeness Index function is designed as follows:

$$S(T) = [f^+(T_{2,out} - T_{2,out,initial})]^2 \tag{12}$$

With a quadratic form, $S(x)$ will have a significantly large value when temperature $T_{2,out}$ is far above the steady-state value. $T_{2,out,initial}$ = 327.98 °C in Eq. (12) is the initial steady-state value of the outlet temperature. Since the steady-state value of outlet temperature $T_{2,out,ss}$ is changing in simulation with varying disturbances d_2 as described in Eq. (9), Eq. (12) is rewritten with deviation variable x_2 as follows:

$$S(x_2(t_{k+N})) = [f^+(x_2(t_{k+N}) + 1616.3(d_2 + \gamma \ \ \Delta d \ \ N))]^2 \tag{13}$$

To avoid high temperature in the methanator, a threshold S_{TH} of Safeness Index function is carefully chosen. Specifically, if the methanator outlet temperature $T_{2,out}$ is constrained below 340 °C, the threshold for $S(x_2)$ is determined to be $(340 - 327.98)^2 = 144.48$. Additionally, the actual threshold used in the controller is chosen to be a conservative value of $S_{TH} = 121$ due to a few intrinsic problems: the model mismatch between the identified model and the real plant, sample-and-hold implementation of the controller and large time delay in the process. A general method to determine the Safeness Index threshold can be found in Albalawi et al. (2017). Based on the Safeness Index function of Eq. (13), the Safeness Index-based MPC is developed as follows:

$$\begin{aligned} \min_{u \in S(\Delta), y} \quad & \int_{t_k + t_{d,2}}^{t_{k+N} + t_{d,2}} (\|\tilde{x}_2(\tau)\|^2_{Q_c}) \ \ d\tau + \int_{t_k}^{t_{k+N}} (\|u_2(\tau)\|^2_{R_c}) \ \ d\tau \\ & + \sum_{i=1}^{N} k_1 e^{-k_2 y(i)}, \quad k_1, k_2 > 0 \end{aligned} \tag{14a}$$

$$\text{s.t. } \dot{\tilde{x}}_2(t) = A_2 \tilde{x}_2(t) + B_2 u_2(t - t_{d,2}) \tag{14b}$$

$$\tilde{x}_2(t_k) = x_2(t_k) \tag{14c}$$

$$u_2(t) = u_{2,pre}(t), \quad \forall t \in [t_k - t_{d,2}, t_k) \tag{14d}$$

$$u_2(t) \in U_2, \quad \forall t \in [t_k, t_{k+N}) \tag{14e}$$

$$S(\tilde{x}_2(t_{k+i} + t_{d,2})) + y(i) \leq S_{TH}, \quad i = 1, 2, \ldots, N \tag{14f}$$

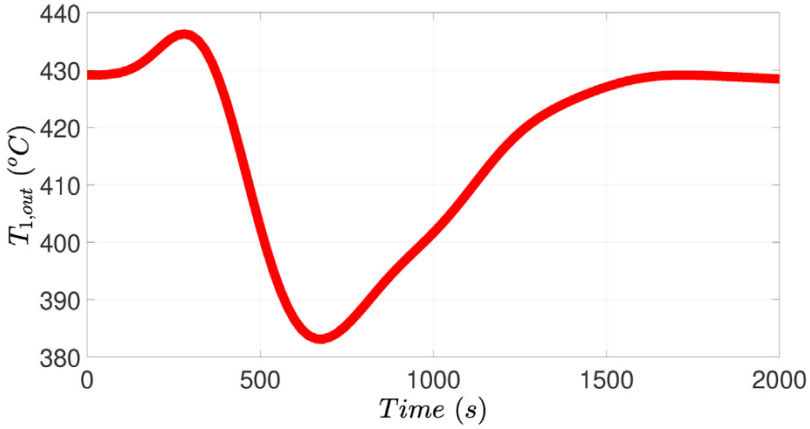

(a) Outlet temperature of the high-temperature shift reactor

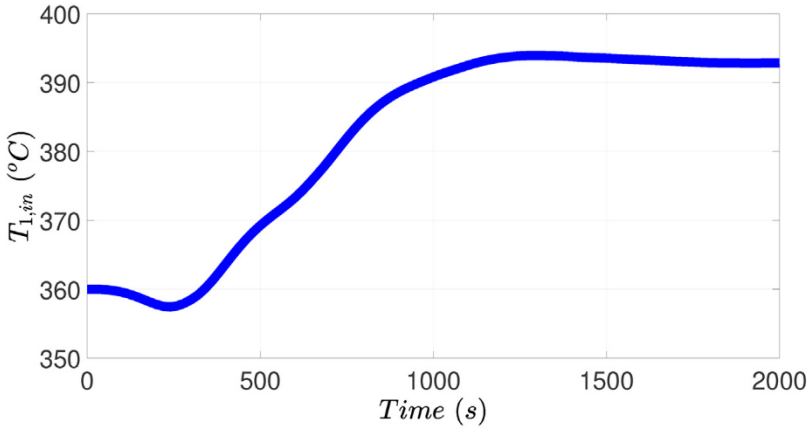

(b) Inlet temperature of the high-temperature shift reactor

Fig. 5 – Closed-loop simulation results under the control structure that uses C_1 and C_2.

Although the optimal input trajectory $u_2^*(t)$ is calculated over the entire prediction horizon $t \in [t_k, t_{k+N})$, the control action computed for the first sampling period in the prediction horizon $u_2(t_k)$ is applied over the first sampling period, and the MPC problem is resolved at the next sampling period. The objective function of Eq. (14a) requires minimizing the integral term $\int_{t_k+t_{d,2}}^{t_{k+N}+t_{d,2}} (\|\tilde{x}_2(\tau)\|_{Q_c}^2)\ d\tau + \int_{t_k}^{t_{k+N}} (\|u_2(\tau)\|_{R_c}^2)\ d\tau$ and the penalty term $\sum_{i=1}^{N} k_1 e^{-k_2 y(i)}$ of slack variables y(i). It is noted that state the is integrated from $t_k + t_{d,2}$ to $t_{k+N} + t_{d,2}$ because states from t_k to $t_k + t_{d,2}$ are already determined by the previously implemented control actions. The constraint of Eq. (14b) is the nominal linear model of Eq. (10) that is used to predict the states of the closed-loop system. Eq. (14c) defines the initial condition $\tilde{x}_2(t_k)$ of the optimization problem which is the state measurement $x_2(t_k)$ at $t = t_k$. Eq. (14d) provides the input trajectory calculated from previous steps, in order to predict the state from t_k to $t_k + t_{d,2}$. Eq. (14e) is the input constraint applied over the entire prediction horizon. The manipulated input is the feed temperature $T_{2,in}$, which is bounded by $180\,^\circ\text{C} \le T_{2,in} \le 380\,^\circ\text{C}$, namely $U_2 = [-100, 100]$. Eq. (14f) is the Safeness Index constraint with slack variables y(i). Since the penalty term $\sum_{i=1}^{N} k_1 e^{-k_2 y(i)}$ is minimized in the objective function, y(i) is maximized so that the Safeness Index is restricted to be below S_{TH} as much as possible. Additionally, the parameters k_1 and k_2 in the objective function of Eq. (14a) should be carefully chosen, such that the slack variables y(i) have a small effect on control actions if $S(x_2(t_k + t_{d,2}))$ is far below S_{TH}, and have a significant effect on control actions if $S(x_2(t_k + t_{d,2}))$ is close to S_{TH} (i.e., approaching the threshold for unsafe operating conditions). Thus, in our simulation k_1 and k_2 are determined to be 10^3 and 0.2, respectively.

The explicit Euler method with an integration time step of $h_c = 10^{-1}$ s was applied to numerically integrate the dynamic model of Eq. (10) in the Safeness Index-based MPC. The nonlinear optimization problem of the Safeness Index-based MPC of Eq. (14) is solved using the solver FilterSD on OPTI Toolbox in Matlab with the following parameters: sampling period $\Delta = 20$ s; prediction horizon $N = 30$. $Q_c = 1$ and $R_c = 2$ are chosen such that the terms of the states and the input have the same order of magnitude in $\|\tilde{x}_2(\tau)\|_{Q_c}^2$ and $\|u_2(\tau)\|_{R_c}^2$.

4. Closed-loop simulation results

4.1. *Simulation results using both C_1 and C_2*

In this section, the performance of the ammonia plant under the proposed controllers C_1 and C_2 is demonstrated. Figs. 5–7 show the closed-loop simulation of the entire ammonia process in the presence of disturbance of catalyst deactivation.

As a result of catalyst deactivation from 1 to 0.2 in the high-temperature shift reactor in the first 300 s, less CO is reacting in the high-temperature shift reactor. After a small inverse response, at about 400 s the outlet temperature of the high-temperature shift reactor starts to decrease below its steady-state value as shown in Fig. 5a. Then, the first controller C_1 measures the decreasing outlet temperature $T_{1,out}$, hence increases the inlet temperature $T_{1,in}$ in order to react more CO in the high-temperature shift reactor, as shown in Fig. 5b. Under the MPC of Eq. (8), the outlet temperature $T_{1,out}$ of

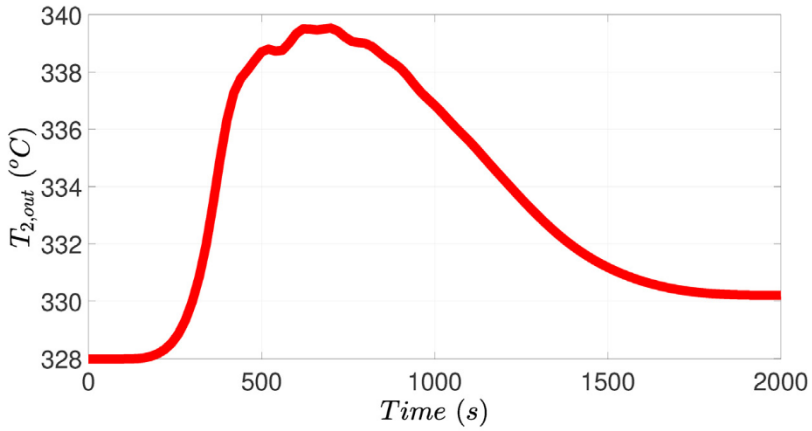

(a) Outlet temperature of the methanator

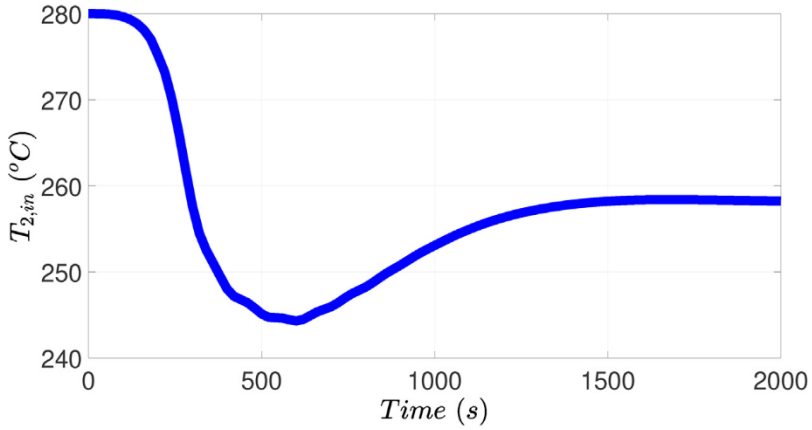

(b) Inlet temperature of the methanator

Fig. 6 – Closed-loop simulation results under the control structure that uses C_1 and C_2.

the high-temperature shift reactor returns back to its steady-state value within 1500 s. Since the catalyst activity in the high-temperature shift reactor has decreased, the reactor is not able to react as much CO as it would have under the initial nominal condition (i.e., without catalyst deactivation), thus more residual unreacted CO leaves the high-temperature shift reactor into the low-temperature shift reactor.

In the next unit of the process, the low-temperature shift reactor mitigates the increased CO content, but a higher concentration of CO (relative to the case of no catalyst deactivation) still leaves the low-temperature shift reactor. Since more CO reaches the methanator, the outlet temperature $T_{2,out}$ from the methanator starts to increase at around 200 s, as shown in Fig. 6a. It is noted that the CO mole fraction y_{CO} in the feed of the methanator is measured at each sampling time t_k and a corresponding steady-state is calculated using Eq. (9). Then, the Safeness Index-based MPC (C_2) measures the outlet temperature $T_{2,out}$ and manipulates inlet temperature $T_{2,in}$ to drive the methanator outlet temperature $T_{2,out}$ to the new steady-state.

In order to understand the influence of the Safeness Index constraint, it is important to mention that the Safeness Index constraint of Eq. (14f) requires all predicted Safeness Index to be below $S_{TH} = 121$ together with the slack variables y(i). When the outlet temperature $T_{2,out}$ gets close to 340 °C at around 500 s as shown in Fig. 6a, S(x) grows close to $S_{TH} = 121$. Because of the Safeness Index constraint of Eq. (14f), small values for slack variables y(i) are used when S(x) is close to S_{TH}, which makes the penalty term $\sum_{i=1}^{N} k_1 e^{-k_2 y(i)}$ dominate the objective function of Eq. (14a). Since the penalty term $\sum_{i=1}^{N} k_1 e^{-k_2 y(i)}$ in the objective function of Eq. (14a) is minimized, slack variables y(i) are optimized to be as large as possible, and thus to restrict the temperature $T_{2,out}$ to be as low as possible. When the outlet temperature $T_{2,out}$ gets far below 340 °C at around 1500 s as shown in Fig. 6a, S(x) is far from $S_{TH} = 121$. Because of the Safeness Index constraint of Eq. (14f), large values for slack variables y(i) are used when S(x) is far from S_{TH}. Large slack variables make the penalty term $\sum_{i=1}^{N} k_1 e^{-k_2 y(i)}$ very small in the objective function of Eq. (14a), and therefore, the Safeness Index constraint of Eq. (14f) can be easily satisfied by choosing large slack variables y(i) without increasing the penalty term $\sum_{i=1}^{N} k_1 e^{-k_2 y(i)}$ in the objective function of Eq. (14a).

Additionally, the Safeness Index constraint of Eq. (14f) and a state constraint are similar especially in this work, but they can be designed with different forms. In general, the Safeness Index can take any formulation that accounts for the impact of multiple process variables, and thus, become more powerful than a simple state constraint. Moreover, soft constraints may be added in the Safeness Index constraint using slack variables, instead of a hard state constraint.

Slack variables y(i) are allowed to choose positive or negative values to meet the constraint of Eq. (14f), depending on the current measurement and the prediction of the state. The main objective of the slack variable is to ensure feasibility of the constraint $S(\tilde{x}_2(t_{k+i} + t_{d,2})) \leq S_{TH}$ when $S(\tilde{x}_2(t_{k+i} + t_{d,2})) > S_{TH}$ for some i. Therefore, slack variables are added in the constraint and are required to be negative when $S(\tilde{x}_2(t_{k+i} + t_{d,2})) > S_{TH}$. The slack variables y(i) allow the Safeness Index to be temporarily above S_{TH} by taking negative slack values, which can be necessary in some scenarios: (a) an abrupt large

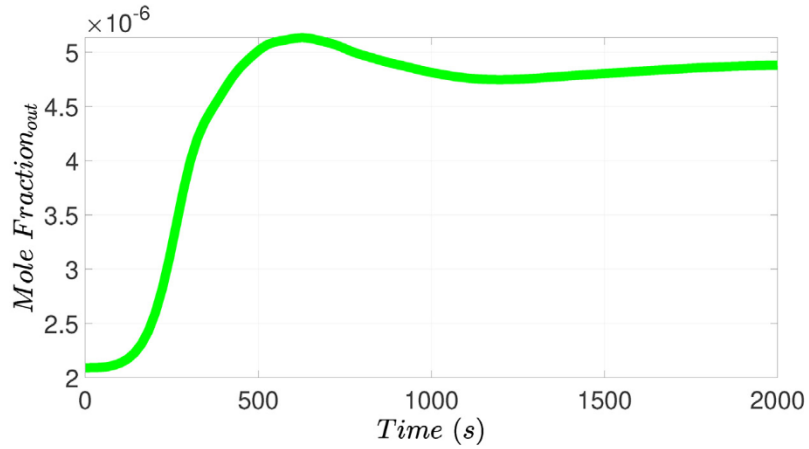

(a) Outlet mole fraction of carbon monoxide of the methanator under the control structure that uses C_1 and C_2.

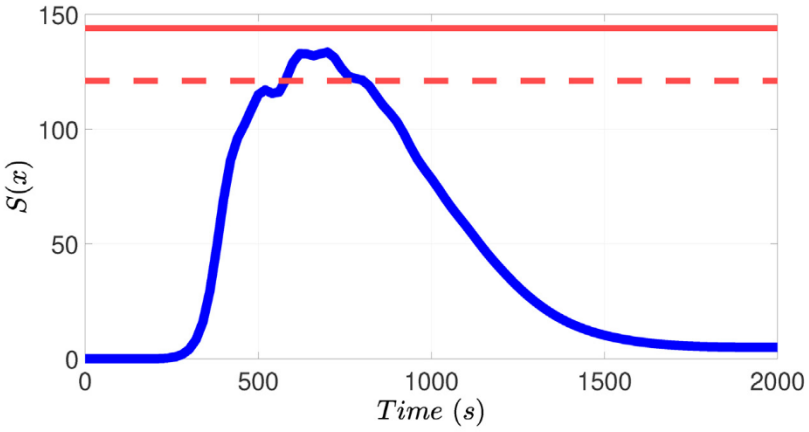

(b) Safeness Index Profile. Solid line is actual process threshold, and dashed line is threshold used in controller.

Fig. 7 – Closed-loop simulation results under the control structure that uses C_1 and C_2.

disturbance occurs so that the outlet temperature exceeds 340 °C very fast; (b) the disturbance d_2 increases very fast so that Δd is very large and the predicted outlet temperature at steady-state $T(t_{k+N})_{out,ss}$ is above 340 °C. If $S(\tilde{x}_2(t_{k+i} + t_{d,2})) \leq S_{TH}$, slack variables are still included in the constraint and are required to be positive. With the help of the slack variables $y(i)$, Fig. 6b demonstrates that the inlet temperature $T_{2,in}$ decreases smoothly when $S(x)$ is close to S_{TH} to avoid the unsafe region, instead of changing abruptly. If the slack variables $y(i)$ were not used in MPC, the inlet temperature $T_{2,in}$ will not start to decrease before the outlet temperature $T_{2,out}$ reaches 340 °C, but will show an abrupt change when the current outlet temperature increases above 340 °C.

Moreover, Fig. 7a shows that the outlet carbon monoxide mole fraction is around 5×10^{-6}, which satisfies the requirements and indicates that the offline calculated steady-state works well. The performance of CO removal in the methanator is not compensated too much by decreasing the methanator inlet temperature in response to the increase in its outlet temperature.

4.2. *Comparison with use of C_2 only*

In this section, the ammonia process is simulated under the same disturbance but with only controller C_2 implemented. Fig. 8 demonstrates the comparison between the simulation results under a single controller C_2 and the simulation results in Section 4.1.

For the scenario that both controllers C_1 and C_2 are used, the first controller C_1 increases the feed temperature $T_{1,in}$ and the reaction rate in the high-temperature shift reactor in order to reduce the effect of reduced catalyst activity. Therefore, the methanator feed CO content will first increase, but eventually decrease after some time delay if the controller C_1 is used. Thus, the controller C_1 mitigates the disturbance d_2 and other unmeasured disturbances to the methanator and finally drives the system to a new steady-state corresponding to a smaller disturbance d_2 in Fig. 8.

However, when only C_2 is used in the ammonia process, the methanator feed CO content increases and remains at a very high level, which introduces a large disturbance d_2 to the methanator. Thus, the controller C_2 drives the methanator to a new steady-state corresponding to a large disturbance d_2. As shown in Fig. 8, the methanator outlet temperature is maintained at around 340 °C if controller C_1 is not used, which is the outlet temperature steady-state when methanator feed CO content is high.

In Fig. 8, it takes more time for two controllers to drive the methanator outlet temperature $T_{2,out}$ to the new steady-state compared to one controller. This is because the high-temperature shift reactor has a larger time delay ($t_{d,1} = 360$ s), therefore the controller C_1 needs a long time to stabilize the high-temperature shift reactor. Then, the methanator feed CO content also decreases slowly and the methanator outlet temperature $T_{2,out}$ needs 2000 s to reach the final steady-state.

4.3. *Comparison with PI controller*

Since proportional-integral (PI) control is still the most popular technique for chemical industries, in this section, the ammonia process is simulated under the same disturbance but with

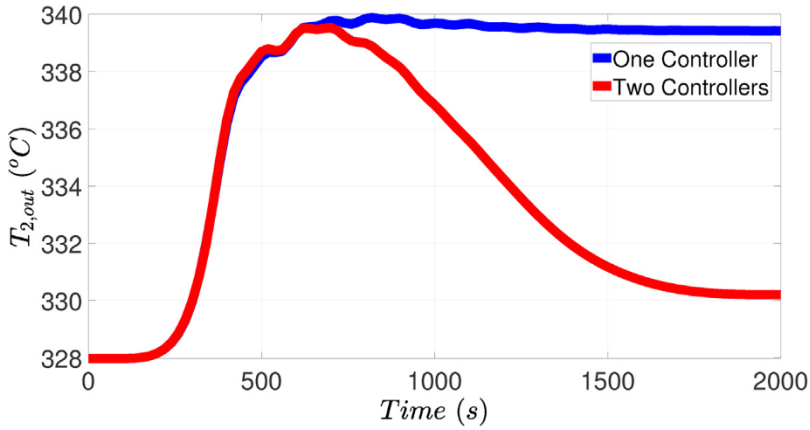

Fig. 8 – Comparison of methanator outlet temperature under two different control schemes: One scenario uses only C_2, and the other scenario uses both C_1 and C_2.

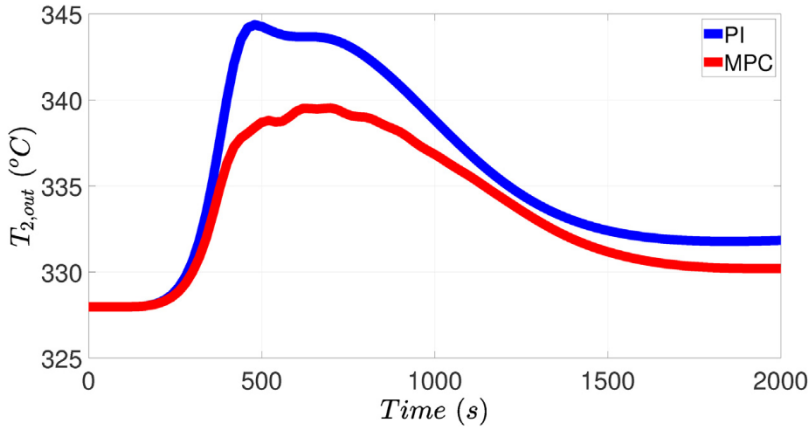

Fig. 9 – Comparison of methanator outlet temperature under PI (both C_1 and C_2) and MPC (both C_1 and C_2) control schemes.

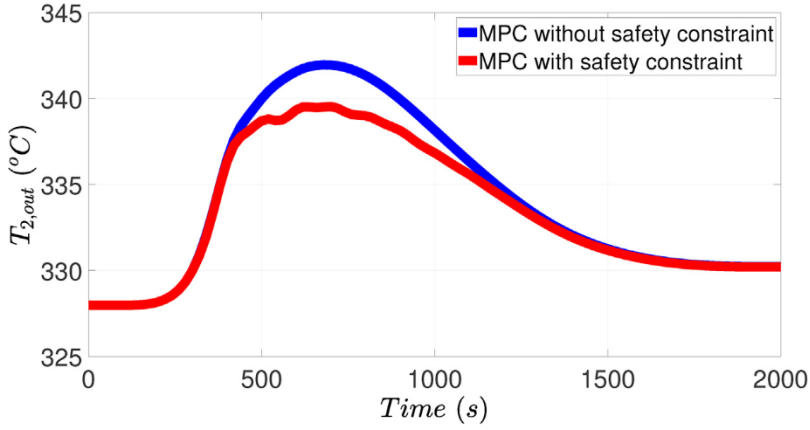

Fig. 10 – Comparison of methanator outlet temperature under MPC with and without Safeness Index constraints.

PI controllers for both C_1 and C_2. Fig. 9 demonstrates the comparison between the simulation results under PI controllers and the simulation results in Section 4.1. Additionally, the PI controller used for C_2 also measure the current disturbance $d_2(t_k)$ and changes the set-point as discussed in Section 3.3.1.

It is noted that state constraints cannot be employed in the PI controllers, but MPC can use Safeness Index constraint of Eq. (14f) to avoid unsafe operations. Moreover, the PI controller cannot account for anticipated future potential increasing disturbance from $d_2(t_{k+1})$ to $d_2(t_{k+N})$, but MPC can consider future disturbance and future steady-state in Eq. (9). Therefore, the closed-loop performance of the PI controller cannot avoid extreme states in the presence of disturbance. Specifically in Fig. 9, the methanator outlet temperature $T_{2,out}$ under the PI controllers goes above 340 °C for a period of 500 s, while the proposed controllers in this paper can avoid exceeding 340 °C.

4.4. *MPC without Safeness Index constraint*

In this section, the ammonia process is simulated under the same disturbance with both C_1 and C_2, in which the Safeness Index constraint of Eq. (14f) is not applied. Fig. 10 demonstrates the comparison between the simulation results under MPC without Safeness Index constraint and the simulation results in Section 4.1.

The objective of controllers is to maintain the methanator outlet temperature $T_{2,out}$ below 340 °C in order to avoid a potential runaway reaction. However, it is observed in Fig. 10 that the MPC without Safeness Index constraint allows the methanator outlet temperature $T_{2,out}$ to be above 340 °C for 400 s. However, due to the Safeness Index constraint of Eq. (14f) that prevents temperature from going extremely high, in the case of the MPC using Safeness Index constraint, the methanator outlet temperature $T_{2,out}$ stays in the safe region of operation for the entire simulation time. This implies that the Safeness Index-based MPC of Eq. (14) can improve process operational safety of the ammonia plant, compared to MPC without Safeness Index constraint.

5. Conclusion

In this work, an application was demonstrated that integrated process operational safety metrics within multiple model predictive controllers for a multi-unit ammonia network. A dynamic simulation was developed in Aspen Plus Dynamics to simulate four units in the industrial ammonia process. A common and problematic disturbance, catalyst deactivation, was introduced into dynamic simulations. The disturbance was first introduced in the high-temperature shift reactor, which propagated from upstream units to downstream units and finally caused dramatic temperature increase in the methanation unit. Two controllers were designed to improve process operational safety in the entire ammonia process network. The first controller was an MPC that controls the high-temperature shift reactor. The second controller was a Safeness Index-based MPC that controls the methanator. Closed-loop simulations demonstrated that extremely high temperature was avoided under the proposed controllers in the presence of significant disturbances.

Acknowledgments

Financial support from the National Science Foundation and the Department of Energy is gratefully acknowledged.

References

Al-Malah, K.I., 2016. Aspen Plus: Chemical Engineering Applications. John Wiley & Sons.
Albalawi, F., Alanqar, A., Durand, H., Christofides, P.D., 2016. A feedback control framework for safe and economically-optimal operation of nonlinear processes. AIChE J. 62, 2391–2409.
Albalawi, F., Durand, H., Alanqar, A., Christofides, P., 2018. Achieving operational process safety via model predictive control. J. Loss Prev. Process Ind. 53, 74–88.
Albalawi, F., Durand, H., Christofides, P.D., 2017. Process operational safety using model predictive control based on a process safeness index. Comput. Chem. Eng. 104, 76–88.
Alhabdan, F., Elnashaie, S., 1995. Simulation of an ammonia plant accident using rigorous heterogeneous models: effect of shift converter disturbances on the methanator. Math. Comput. Model. 21, 85–106.
Appl, M., 2000. Ammonia, Ullmann's Encyclopedia of Industrial Chemistry. Wiley Online Library.
Araújo, A., Skogestad, S., 2008. Control structure design for the ammonia synthesis process. Comput. Chem. Eng. 32, 2920–2932.
Argyle, M., Bartholomew, C., 2015. Heterogeneous catalyst deactivation and regeneration: a review. Catalysts 5, 145–269.
Aspen Technology, Inc, 2003. Aspen Plus User Guide, Cambridge, MA.
Aspen Technology, Inc, 2017. Aspen Plus Ammonia Model, Bedford, MA.
Bø, T.I., Johansen, T.A., 2014. Dynamic safety constraints by scenario based economic model predictive control. Proceedings of the IFAC World Congress, Cape Town, South Africa, 9412–9418.
Campbell, J., 1970. Influences of catalyst formulation and poisoning on the activity and die-off of low temperature shift catalysts. Ind. Eng. Chem. Process Des. Dev. 9, 588–595.
Czuppon, T., Knez, S., Rovner, J., 1992. Ammonia, Kirk-Othmer Encyclopedia of Chemical Technology. Wiley Online Library.
Domanski, P.D., Golonka, S., Jankowski, R., Kalbarczyk, P., Moszowski, B., 2016. Control rehabilitation impact on production efficiency of ammonia synthesis installation. Ind. Eng. Chem. Res. 55, 10366–10376.
Ettouney, H.M., Shaban, H.I., Nayfeh, L.J., 1995. Theoretical analysis of high and low temperature shift converters. Chem. Eng. Commun. 134, 1–16.
Janošovský, J., Danko, M., Labovský, J., Jelemenský, L., 2017. The role of a commercial process simulator in computer aided HAZOP approach. Process Saf. Environ. Prot. 107, 12–21.
Khorsand, K., Marvast, M., Pooladian, N., Kakavand, M., 2007. Modeling and simulation of methanation catalytic reactor in ammonia unit. Pet. Coal 49, 46–53.
Kohl, A., Nielsen, R., 1997. Gas Purification. Gulf Publishing Co., Houston, USA.
Lao, L., Ellis, M., Christofides, P.D., 2013. Proactive fault-tolerant model predictive control. AIChE J. 59, 2810–2820.
Luyben, W.L., 2012. Use of dynamic simulation for reactor safety analysis. Comput. Chem. Eng. 40, 97–109.
Luyben, W.L., 2018. Plantwide control of a coupled reformer/ammonia process. Chem. Eng. Res. Des. 134, 518–527.
Martínez, I., Armaroli, D., Gazzani, M., Romano, M., 2017. Integration of the Ca-Cu process in ammonia production plants. Ind. Eng. Chem. Res. 56, 2526–2539.
Mhaskar, P., Liu, J., Christofides, P.D., 2013. Fault-Tolerant Process Control: Methods and Applications. Springer-Verlag, London, England.
Nayak-Luke, R., Bañares-Alcántara, R., Wilkinson, I., 2018. Green ammonia: impact of renewable energy intermittency on plant sizing and levelized cost of ammonia. Ind. Eng. Chem. Res. 57, 14607–14616.
Ocampo, R., 1996. Examination of methanation vessel after overheating – a case study. Mater. Corros. 47, 392–396.
Ojha, M., Dhiman, A., 2010. Problem, failure and safety analysis of ammonia plant: a review. Int. Rev. Chem. Eng. 2, 631–646.
Papazoglou, I., Aneziris, O., 2003. Master logic diagram: method for hazard and initiating event identification in process plants. J. Hazard. Mater. 97, 11–30.
Pattabathula, V., Richardson, J., 2016. Introduction to ammonia production. Chem. Eng. Prog. 112, 69–75.
Peng, P., Nguyen, H., Harold, M., Luss, D., 2017. Spatio-temporal phenomena in monolithic reactors measured by combined spatially-resolved mass spectrometry and optical frequency domain reflectometry. In: Advances in Chemical Engineering, vol. 50. Elsevier, pp. 83–130.
Rahimpour, M., Dehnavi, M., Allahgholipour, F., Iranshahi, D., Jokar, S., 2012. Assessment and comparison of different catalytic coupling exothermic and endothermic reactions: a review. Appl. Energy 99, 496–512.
Rönsch, S., Schneider, J., Matthischke, S., Schlüter, M., Götz, M., Lefebvre, J., Prabhakaran, P., Bajohr, S., 2016. Review on methanation-from fundamentals to current projects. Fuel 166, 276–296.
Rounthwaite, D., 1983. Improved ammonia plant catalysts. Pressure drop can be minimized using appropriately sized reforming catalysts, water-resistant high-temperature shift catalysts, and a new generation of low-temperature shift catalysts. Process Saf. Prog. 2, 127–131.
Seo, Y., Seo, D., Seo, Y., Yoon, W., 2006. Investigation of the characteristics of a compact steam reformer integrated with a water-gas shift reactor. J. Power Sources 161, 1208–1216.

Shah, M., 1967. Control simulation in ammonia production. Ind. Eng. Chem. 59, 72–83.
Shah, M.J., Weisenfelder, A.J., 1969. Control and optimization of a large ammonia plant with a digital computer. Automatica 5, 319–333.
Twigg, M., 1989. Catalyst Handbook. Wolfe Publishing Ltd., London.
Van Dijk, H., Boon, J., Nyqvist, R., Van Den Brink, R., 2010. Development of a single stage heat integrated water-gas shift reactor for fuel processing. Chem. Eng. J. 159, 182–189.
Walton, M., Southerton, T., Sharp, P., 2009. Safety Improvements in a Methanation Reactor, Process Safety Progress. Wiley Online Library.
Wu, Z., Durand, H., Christofides, P.D., 2018. Safe economic model predictive control of nonlinear systems. Syst. Control Lett. 118, 69–76.
Zhang, C., Vasudevan, S., Rangaiah, G., 2010. Plantwide control system design and performance evaluation for ammonia synthesis process. Ind. Eng. Chem. Res. 49, 12538–12547.
Zhang, S., Tong, J., Zhao, J., 2016. An integrated modeling approach for event sequence development in multi-unit probabilistic risk assessment. Reliab. Eng. Syst. Saf. 155, 147–159.
Zhang, Z., Wu, Z., Durand, H., Albalawi, F., Christofides, P.D., 2018. On integration of feedback control and safety systems: analyzing two chemical process applications. Chem. Eng. Res. Des. 132, 616–626.
Zhang, Z., Wu, Z., Rincon, D., Garcia, C., Christofides, P.D., 2019. Operational safety of chemical processes via safeness-index based MPC: two large-scale case studies. Comput. Chem. Eng. 125, 204–215.